Journal of Nuclear Medicine, published on March 15, 2019 as doi:10.2967/jnumed.118.219766

IMAGING THE ENZYME 11β-HYDROXYSTEROID DEHYDROGENASE TYPE 1 WITH POSITRON EMISSION TOMOGRAPHY: EVALUATION OF THE NOVEL RADIOTRACER ^{11}C-AS2471907 IN HUMAN BRAIN

Jean-Dominique Gallezot[1], Nabeel Nabulsi[1], Shannan Henry[1], Richard Pracitto[1], Beata Planeta[1], Jim Ropchan[1], Shu-Fei Lin[1], David Labaree[1], Michael Kapinos[1], Anupama Shirali[1], Teresa Lara-Jaime[1], Hong Gao[1], David Matuskey[1], Mark Walzer[2], Gerard J. Marek[2], Susan Bellaire[3], Nancy Yuan[4], Richard E. Carson[1], Yiyun Huang[1].

[1]Department of Radiology and Biomedical Imaging, Yale University School of Medicine, New Haven, CT, United States.
[2]Astellas Pharma Global Development, Northbrook, IL, United States
[3]Astellas Pharma Europe BV, Leiden, Netherlands
[4]Astellas Pharma Global Development, Northbrook, IL, United States

Corresponding author:

Jean-Dominique Gallezot
e-mail: jean-dominique.gallezot@yale.edu
phone: 203-785-7271
fax: 203-785-3107
address: Yale University PET Center, 801 Howard Ave, PO Box 208048, New Haven, CT 06520-8048

Words: 5484 / 5000

Running title: 11β-HSD1 brain imaging

ABSTRACT

The 11β-hydroxysteroid dehydrogenase type 1 (11β-HSD1) enzyme converts cortisone to cortisol, and participates in the regulation of glucocorticoid levels in tissues. 11β-HSD1 is expressed in the liver, kidney, adipose, placenta and brain. 11β-HSD1 is a target for treatment of depression, anxiety, post-traumatic stress disorder, and also against age-related cognitive function and memory loss. In this study, we evaluated the radiotracer ^{11}C-AS2471907 (3-(2-chlorophenyl)-4-(methyl-^{11}*C*)-5-[2-[2,4,6-trifluorophenoxy]propan-2-yl]-4*H*-1,2,4-triazole) to image 11β-HSD1 availability in the human brain with PET. **Methods:** Fifteen subjects were included in the study. All subjects underwent one two-hour scan following a bolus administration of ^{11}C-AS2471907. Two subjects underwent an additional scan following blockade with the selective and high affinity 11β-HSD1 inhibitor ASP3662 to evaluate ^{11}C-AS2471907 non-displaceable distribution volume (V_{ND}). Five subjects also underwent an additional scan to evaluate the within-day test-retest variability of ^{11}C-AS2471907 volumes of distribution (V_T). **Results:** ^{11}C-AS2471907 time-activity curves were best fitted by the two-tissue compartment (2TC) model. ^{11}C-AS2471907 exhibited a regionally-varying pattern of uptake throughout the brain. The volume of distribution of ^{11}C-AS2471907 ranged from 3.7 ± 1.5 mL/cm^3 in the caudate nucleus to 14.5 ± 5.3 mL/cm^3 in the occipital cortex, with intermediate values in the amygdala, white matter, cingulum, insula, frontal cortex, putamen, temporal and parietal cortices, cerebellum, and thalamus (from lowest to highest V_T). From the blocking scans, V_{ND} was determined to be 0.16 ± 0.04 mL/cm^3 for ^{11}C-AS2471907. Thus, nearly all uptake was specific and the binding potential (BP_{ND}) ranged from 22 in the caudate to 90 in the occipital cortex. Test-retest variability of 2TC V_T values was <10% in most large cortical regions (14% in parietal cortex) and ranged from 14% (cerebellum) to 51% (amygdala) in other regions. Intraclass correlation coefficient of 2TC V_T values ranged from 0.55 in the white

matter to 0.98 in the cerebellum. **Conclusion:** ^{11}C-AS2471907 has a very high fraction of specific binding *in vivo* in humans, and reasonable within-day reproducibility of binding parameters.

Keywords: 11β-Hydroxysteroid dehydrogenase-1, Cortisol, Brain, Positron Emission Tomography.

INTRODUCTION

The hypothalamus, pituitary gland, and adrenal gland collectively form a complex circuit of direct influences and feedback interactions called the HPA axis. This is a major part of the neuroendocrine system and controls the response to stress and modulates a variety of processes, including digestion, mood, emotion, immune reaction, sexuality, and energy storage and consumption. Stress induces the activation of the HPA axis and release of glucocorticoids. Two enzymes are involved in the regulation of glucocorticoids and activation of glucocorticoid receptors: 11β-hydroxysteroid dehydrogenase-1 (11β-HSD1), a reductase *in vivo* that converts cortisone to cortisol and amplifies glucocorticoid action in a tissue-specific manner, and 11β-hydroxysteroid dehydrogenase-2 (11β-HSD2) that catalyzes the conversion of cortisol back to cortisone. 11β-HSD1 is expressed in the liver, kidney, adipose tissue, placenta and brain, while 11β-HSD2 is primarily expressed in the kidney and functions mainly as a source of cortisone production. Together, glucocorticoid homeostasis is maintained by the HPA axis and activities of the 11β-HSD enzymes.

In the rodent brain, 11β-HSD1 activity is highest in the cerebellum, hippocampus, and neocortex, with levels about 10-30% of those in kidney and liver (*1-3*). Activity in other regions of the brain are also detected, including the anterior pituitary, hypothalamus, amygdala and brain stem (*1,3,4*). A similar expression pattern is found in the post-mortem human brain (*5*). In general, the pattern of 11β-HSD1 mRNA expression in the brain is paralleled by those of immunohistochemistry and enzyme activity. Since 11β-HSD1 is expressed in key brain regions in the negative feedback action of glucocorticoids, this enzyme is a critical regulator of the HPA axis (*6*), and thus important in the pathophysiology of stress-related disorders such as depression,

post-traumatic stress disorder and addictive behaviors, where dysregulation of the HPA axis and glucocorticoids has been abundantly demonstrated (*7-9*). In addition to these disorders, accumulating evidence has pointed to the association of age-related cognitive impairment, elevated glucocorticoid levels, and increased 11β-HSD1 expression in the brain (*10-12*). Inhibition of 11β-HSD1 has been shown to improve memory (*13*), and to protect against the decline of cognitive function with age (*5,14-16*), or the even more catastrophic memory loss associated with Alzheimer's disease (AD) (*17*). Importantly, recent evidence appears to also indicate a link between insulin resistance and AD (*18*). As a result, 11β-HSD1 inhibitors, originally targeted for type 2 diabetes, have been proposed as a target for drug development to treat cognitive impairment.

Positron Emission Tomography (PET) is a powerful imaging technology for the *in vivo* investigation of biological targets. The availability of PET imaging agents for 11β-HSD1 will provide non-invasive biomarkers to interrogate the enzyme *in vivo* in human subjects and gain insights into its function and dysfunction in diseases. Further, PET imaging with 11β-HSD1 radiotracers can be used to assess target engagement and correlate target occupancy, dose exposure and therapeutic response of 11β-HSD1 inhibitors currently in clinical trials, thus aiding the development of novel therapeutic agents. Merck was the first to disclose a PET radiotracer for imaging 11β-HSD1 in the brain, and ligand ^{11}C-**1** (Fig. 1) was reported in a conference abstract as having good brain uptake in rhesus monkeys and specific binding *in vivo* that could be blocked by MK-0916, a selective 11β-HSD1 inhibitor (*19*). However, imaging studies in humans with this radiotracer have not been reported. We have previously reported ^{11}C-AS2471907 (**2**) (Fig. 1), with K_i of 2.2 nM for 11β-HSD1, >10 μM for 11β-HSD2, and minimal binding affinity for a wide range of protein targets, as a suitable PET radiotracer to image the

11β-HSD1 in the monkey brain. Here, we report the first PET imaging evaluation of ^{11}C-AS2471907 in humans to 1) assess its pharmacokinetic characteristics, 2) select the optimal method for quantitative analysis, 3) examine the test/retest reproducibility of kinetic and in vivo binding parameters, and 4) define the levels of specific binding via blocking studies.

MATERIALS AND METHODS

Study Plan and Population

The study was conducted in compliance with the ethical principles originating in or derived from the Declaration of Helsinki and in compliance with all International Conference on Harmonization (ICH) Good Clinical Practice (GCP) guidelines. In addition, all local regulatory requirements were followed, in particular, those affording greater protection to the safety of trial participants. These studies were performed under protocols approved by the Yale School of Medicine Human Investigation Committee, the Yale-New Haven Hospital Radiation Safety Committee, and the Yale University Radiation Safety Committee. Subjects were recruited by public advertisement. Written informed consent was obtained from all participants after full explanation of study procedures. Dosing of ASP3662 was conducted under the Astellas IND (IND 116,896).

All subjects were healthy males and had a comprehensive screening assessment that included a clinical interview, complete physical examination with medical history, routine blood tests, electrocardiogram (ECG) and urine toxicology. Individuals were excluded if they self-reported or evaluation revealed a diagnosis of a current and/or lifetime psychiatric disorder; a history of suicide attempts, current or past serious medical or neurological illness (including a history of head injury with loss of consciousness); a history of substance abuse or dependence; nicotine use in the past 6 months; prescription or non-prescription medication in the last two weeks or clinically significant lab or ECG results.

Fifteen subjects were included in the study (age: 38 ± 8 y, range: 28 - 51 y; body weight: 84 ± 9.7 kg, range: 69 - 100 kg). Two subjects underwent an additional scan after pre-blockade

of 11β-HSD1 by ASP3662 (*20*) (30 mg, 26 ± 3 h before tracer injection), and five subjects underwent a second (retest) scan on the same day to assess test-retest variability. Test scans occurred between 10 AM and 3 PM, and retest scans occurred 2.7 to 6.4 h later.

Radiochemistry

The reference standard AS2471907 and its *N*-desmethyl triazole precursor AS319448 were provided by Astellas Pharma Inc., Japan. ^{11}CO2 was produced with the PETTrace cyclotron (GE Healthcare) through the ^{14}N(p,α)^{11}C nuclear reaction by bombarding a high-pressure nitrogen target containing 1% oxygen with a 16.8-MeV proton beam.

The radiotracer ^{11}C-AS2471907 was prepared by *N*-^{11}C-methylation of the precursor AS319448-00 (10 mg) with ^{11}C-methyl triflate in anhydrous acetonitrile (0.2 mL) at 70 °C for 5 min (Fig. 2) using the TRACERlab FXC Pro automated synthesis module (GE Healthcare, Milwaukee, WI, USA). The crude reaction mixture was purified by high-performance liquid chromatography (HPLC) (YMC-pack Pro C18 column, 5 μm, 250 × 10 mm, YMC America Inc., Allentown, PA). The column was eluted with a solvent mixture of 45% acetonitrile, 5% THF, and 50% 0.04 M HCl (v/v, pH 1.4) at a flow rate of 4 mL/min and monitored by UV and radioactivity detectors. The desired radioactive product was collected, diluted with 50 mL of de-ionized water, and passed through a Waters C18 SepPak cartridge. The cartridge was rinsed with 10 mL of 0.001 N HCl. The radioactive product was eluted off the SepPak with 1 mL of absolute ethanol (USP) followed by 3 mL of saline (USP), and collected into the FXC Pro product vial. Finally, the combined product solution was passed through a sterile 0.22 μm membrane filter for terminal sterilization and collected into a pyrogen-free collection vial precharged with 7 mL of

saline (USP) and 40 μL of 4.2% sodium bicarbonate solution (USP) to afford a formulated solution ready for dispensing and administration.

Radiochemical purity and molar activity were determined by HPLC analysis of the final product solution (column: Phenomenex Luna C18(2), 5 μm, 4.6 x 250 mm; mobile phase: 52% of acetonitrile and 48% of 0.1 M aqueous ammonium formate solution containing 0.5% acetic acid, pH 4.2; flow rate: 2 mL/min; UV detector wavelength: 230 nm).

PET Data Acquisition

PET scans were performed on the HRRT scanner (resolution 2.5-3 mm FWHM) for 120 min. During the scans, subjects wore an optical tracking tool to record head motion with an infrared detector (Vicra, NDI Systems, Waterloo, Ontario, Canada). PET data were reconstructed with all corrections including motion (as recorded by the Vicra) using the ordered subset-expectation maximization algorithm (2 iterations, 30 subsets).To correct any residual motion due to possible slippage of the tracking tool on the subject's head, a second step of motion correction was applied to the dynamic images, using a mutual-information algorithm (FSL-FLIRT version 3.2, Analysis Group, FMRIB, Oxford, UK) with frame-by-frame registration to a summed image (0-10 min).

Arterial Blood Measurements

Arterial blood samples were drawn from a catheter inserted in the radial artery to measure the whole blood and plasma radioactivity curves, the metabolite corrected plasma curve and the plasma free fraction as previously described (*21,22*), with modifications for the HPLC methods. In brief, plasma analysis of the radiotracer metabolism was performed from samples collected at 3, 8, 15, 30, 60, 90 min. The automatic column-switching HPLC system was equipped with a

capture column (19 × 4.6 mm) packed with Phenomenex SPE Strata-X sorbent (Torrance, CA, USA) and a Phenomenex Luna phenyl-hexyl analytical column (5 μm, 250 × 4.6 mm) with a mobile phase composed of 55% of acetonitrile and 45% of 50 mM ammonium acetate (v/v) at a flow rate of 1.55 mL/min. The retention time for ^{11}C-AS2471907 was ~11 min.

Computation of Time-Activity Curves (TACs)

Each subject underwent one Magnetic Resonance (MR) scan as previously described (*23*) to help analyze the PET data. Then, 13 regions of interest (ROIs) were selected from the Anatomical Automatic Labeling (AAL) template for SPM2 (*24*) in the centrum semiovale, amygdala, caudate nucleus, putamen, thalamus, cerebellum, cingulate, insula, frontal cortex, occipital cortex, parietal cortex and temporal cortex and were applied to the PET data to generate TACs using each subject's MR image to co-register the template and the PET data (*23*).

Kinetic Modeling

Volume of distribution (V_T) (*25*) values were estimated using the one- and two-tissue compartment models (*26*). Both models included a blood volume term, with a fitted vascular fraction. In pre-block studies, the occupancy of the target enzyme and the non-displaceable volume of distribution (V_{ND}) were computed using the occupancy plot (*27*). The variability of V_T values was assessed by computing the intraclass correlation coefficient (ICC) (*28*) and the test-retest variability (TRV), with TRV = $2 \times (V_T^{retest} - V_T^{test})/(V_T^{test} + V_T^{retest})$. The mean of TRV values (mTRV) across subjects is an index of the trend between the test and retest scans. The standard deviation of TRV (sdTRV) is an index of the variability in V_T estimates.

Unless otherwise specified, data are presented as mean ± standard deviation across the 15 baseline scans (first scan for each subject).

RESULTS

The radiotracer ^{11}C-AS2471907 was produced in radiochemical purity of 99.3% ± 0.5% (minimum: 98.4%, *n* = 22), with molar activity 190 ± 239 MBq/nmol (range: 44-1,210 MBq/nmol) at the end of synthesis.

The injected activity dose was 234 ± 114 MBq (range: 94 - 440 MBq) for of ^{11}C-AS2471907, with administered mass of 2.5 ± 2.6 μg (range: 0.25 - 9.7 μg). There were no adverse or clinically detectable pharmacologic effects in any of the 15 subjects. No significant changes in vital signs, laboratory results or electrocardiograms were observed.

Input Functions

The parent fraction remained high through the two-hour scan: 95% ± 3% at 30 min and 85% ± 15% at 90 min after ^{11}C-AS2471907 injection (Supplemental Fig. 1). Administration of the 11β-HSD1 inhibitor ASP3662 led to lower parent fractions: 81% ± 8% at 30 min and 66% ± 13% at 90 min (n=2). At baseline, the standard uptake value (SUV) of ^{11}C-AS2471907 in the plasma peaked at 23 ± 5 at the end of the injection, and then decreased to 0.08 ± 0.02 at the end of the scan. The plasma clearance rate of ^{11}C-AS2471907 was 1.0 ± 0.21 L/min. The plasma concentration of ^{11}C-AS2471907 increased with pre-administration of ASP3662 (Fig. 3): at the end of the scan, the plasma SUV was 1.1 ± 0.7, and the plasma clearance rate decreased to 0.21 ± 0.10 L/min (n=2). Thus, blockade of the enzyme by the 11β-HSD1 inhibitor ASP3662 dramatically slowed clearance and increased tracer bioavailability. The plasma free fraction of ^{11}C-AS2471907 was measured at 1.6% ± 0.5% at baseline and 1.4% ± 0% after ASP3662 administration. The whole blood to plasma ratio was constant at 0.63±0.07 for all timepoints and studies, indicating that the radiotracer and its metabolites do not enter blood cells.

Brain PET Images

Representative images of ^{11}C-AS2471907 in the brain are shown in Fig. 4 and in Supplemental Fig. 2. The rank order of regional binding, from lowest to highest peak uptake, was: white matter, caudate, amygdala, insula, cingulum, frontal and temporal cortices, putamen, cerebellum, parietal cortex, thalamus and occipital cortex. In the occipital cortex, SUV peaked at 2.7 ± 0.4 at ~ 60 min and then decreased to 2.4 ± 0.5 at 120 min. In the white matter region, the peak SUV was 1.0. ± 0.2. After administration of ASP3662, ^{11}C-AS2471907 uptake was reduced dramatically in the brain, especially in regions with higher uptake at baseline: in the occipital cortex, the SUV peaked at 1.2 ± 0.2 at ~ 2 min and then decreased to 0.3 ± 0.1 at the end of the scan. Representative TACs at baseline and after blockade are shown in Fig. 3 and Supplemental Fig. 3.

Kinetic Modeling

Representative fits of regional TACs with the 1TC and 2TC models are shown in Fig. 5. According to the F-test, the 2TC model produced better fits ($F_{2,28}>3.34$, $p<0.05$) than the 1TC model in most cases (171 out of 240 baseline fits, and 24 out of 24 post-drug fits). At baseline, 2TC V_T values ranged from 3.7 ± 1.5 mL/cm^3 (range: 2.1 - 7.2 mL/cm^3) in the caudate nucleus to 14.5 ± 5.3 mL/cm^3 (range: 7.8 - 28 mL/cm^3) in the occipital cortex (Table 1). There was large variability in V_T values across subjects. The coefficient of variation (COV) across subjects ranged from 35% in the centrum semiovale (white matter region) to 52% in the cerebellum. The relative standard error (rSE) on V_T estimates was typically lower than the COV: for the 2TC the median rSE ranged from 3% in the frontal cortex to 34% in the amygdala. The entry rate constant (K_1) was low: the median 2TC K_1 value ranged from 0.022 mL/min/cm^3 in the centrum semiovale to 0.070 mL/min/cm^3 in the thalamus. Though the 2TC model produced better fits in

most cases, the V_T values obtained with the 1TC and 2TC models were highly correlated (r^2=0.984), with a slope close to one (0.977) and an intercept close to zero (-0.545). A Bland-Altman plot comparing 2TC and 1TC V_T values is shown in Fig. 6. The high correlation between 2TC and 1TC V_T values may be in part explained by the fact that the fit in the 1TC was poor only in the early frame data, and became better in the later data (Fig. 5).

After administration of ASP3662, regional V_T values were drastically reduced, and ranged from 0.16 ± 0.01 mL/cm^3 in the amygdala to 0.23 ± 0.07 mL/cm^3 in the occipital cortex (Supplemental Table 1). Occupancy plots for the two blockade scans with ASP3662 are shown in Fig. 7. The occupancy was > 99% in both scans, and the non-displaceable volume of distribution (V_{ND}) was estimated at 0.16 ± 0.04 mL/cm^3. Thus, virtually all tracer uptake in the baseline scans is specifically bound. Based on this V_{ND} estimate and the mean baseline 2TC V_T estimates, regional binding potential (BP_{ND}) of ^{11}C-AS2471907 was calculated and ranged from 22 in the caudate to 90 in the occipital cortex. However, given the very low V_{ND}, it is likely that BP_{ND} estimates may not be that reliable.

Test-retest summary statistics are presented in Table 2, and individual scan V_T values are shown in Supplemental Table 2. During the retest scan, ^{11}C-AS2471907 V_T values tended to be higher than those from the test scan: the average TRV value (mTRV) was positive in most regions and models. Without correction for multiple comparisons, the difference between V_T values was significant in a few regions (paired Student t-test, p<0.05): the cingulum, insula, and the frontal, occipital and temporal cortices (for the 2TC model). With the 2TC model, sdTRV was <10% in most cortical ROIs (14% in the parietal cortex) and ranged from 14% (cerebellum) to 51% (amygdala) in other ROIs. ICC values ranged from 0.55 in the centrum semiovale to 0.98 in the cerebellum, indicating that the large intersubject variability in V_T was not caused by

measurement error. Comparing methods, the 2TC model produced the lowest median (across all ROIs) mTRV and sdTRV values, indicating that the simpler model did not produce less variable V_T estimates.

The effect of scan duration is presented in Supplemental Table 3. If the scan duration is reduced to 90 min, the mean bias on 2TC V_T values is on the order of 8% (median value across all ROIs), but up to 31% in small ROIs; the bias standard deviation is on the order of 8% (median value across all ROIs), but up to 58% in the smallest ROIs. Test-retest variability (sdTRV) is also increased by 10 percentage points (median value across all ROIs) when using only 90 min of data.

DISCUSSION

In this study, we evaluated the novel radiotracer ^{11}C-AS2471907 to quantify the distribution of the 11β-HSD1 enzyme in the brain of healthy human subjects.

The parent fraction of ^{11}C-AS2471907 in plasma remained relatively high through the scans, although clearance of ^{11}C-AS2471907 from the plasma was fast. Following blockade of 11β-HSD1, plasma concentration of ^{11}C-AS2471907 increased, and the parent fraction decreased, as also seen with tracers for other targets such as serotonin transporters with large number of binding sites in the periphery (*29*). At baseline, uptake in the brain, as measured by SUVs, ranged from 1 to 2.5, which is sufficient for imaging studies. ^{11}C-AS2471907 V_T values were well correlated with mRNA scores for the 11ß-HSD1 gene in the Allen human brain atlas (probes 1027298 and 1027299) in the cortex (r>0.92, n=6, p<0.01), and in all ROIs excluding the white matter ROI (centrum semiovale) (r>0.81, n=11, p<0.002). The white matter has the highest 11ß-HSD1 mRNA expression in the Allen atlas, which does not match the present results.

Kinetic modeling indicated that the 2TC provided better fits than the 1TC model. Moreover, the test-retest study indicated that the V_T estimates tended to be less variable with the 2TC than with the 1TC model. Based on these observations, the 2TC model is the recommended method for quantification of ^{11}C-AS2471907 V_T values. Due to the low uptake rate constant (K_1 <0.1 mL/min/cm^3), it is also recommended to include a blood volume correction term in the model and to estimate the vascular fraction for each ROI. The low K_1 values may be due in part to the low plasma free fraction for this tracer (~1.5%). A reference tissue model is not appropriate for this radiotracer, and likely not appropriate for any tracer targeting 11β-HSD1 due to the ubiquitous distribution of 11β-HSD1 in brain.

Since the baseline TACs were relatively flat (Fig. 3A), near-equilibrium conditions might be reached. Therefore, to evaluate if kinetic modeling could be avoided, the tissue to metabolite-corrected plasma ratio (SUVR) was computed (at 60-90 min) and compared to V_T. SUVR tended to be larger than V_T in all ROIs: e.g., it was 67% ± 48% higher in the occipital cortex. Moreover, the test-retest variability of SUVR also tended to higher than that of V_T: e.g., sdTRV was 5% for V_T and 16% for SUVR in the occipital cortex. Overestimation of V_T by SUVR is expected unless washout from tissue is much faster than that from plasma (*30*), and SUVR is additionally sensitive to the variability of these two parameters.

Blocking studies indicated that ^{11}C-AS2471907 has specific binding in all investigated ROIs and thus that there is no reference region for this target. Moreover, ^{11}C-AS2471907 non-displaceable volume of distribution was very low compared to baseline V_T values, indicating that most of the tracer uptake in the brain is due to specific binding.

There was a large range of 11C-AS2471907 V_T values across subjects. This difference between subjects was confirmed during the retest scans as indicated by the high ICC values for V_T estimates. The test-retest studies also indicated that V_T values from the retest scans tended to be higher than those from the test scans done earlier on the same day. This trend apparently needs verification in future studies. Nonetheless, based on the current data, care should be taken in the planning of these future studies to account for this possibility. These changes in V_T values could be diurnal, or habituation of the subjects to the PET procedures. Diurnal changes in cortisol levels in the periphery are well documented (*31*), however it is not yet known if such changes occur for 11β-HSD1 in the brain. The test-retest variability was low in large cortical ROIs (<10%) but higher in smaller ROIs. This is in part due to the low injected activity dose in

these studies (234 MBq in average), leading to noisier images and data. AS2471907 is amenable to radiolabeling with fluorine-18, which is expected to improve image quality and quantification.

The recommended scan duration based on the present data is 120 min, due to increased variability of V_T estimates with shorter scans. In the future, shorter scan length may be possible if injected activity doses can be increased, or if the fluorinated version of this tracer is used.

As the first 11β-HSD1 PET radiotracer for human use, ^{11}C-AS2471907 should be useful for measuring target occupancy by 11β-HSD1 inhibitors in the brain. Secondly, this radiotracer can be used to compare brain occupancy by 11β-HSD1 inhibitors to functional activity of 11β-HSD1 in the brain (CSF measurements) or periphery in order to explore single dose or multiple dose exposure relationships and inform optimal dose selection for clinical trials. Third, quantification of 11β-HSD1 with ^{11}C-AS2471907 would allow the investigation of whether stress-related or other diseases alter 11β-HSD1 protein expression in the brain.

CONCLUSION

This is the first report of a PET radiotracer to image and quantify the enzyme 11β-HSD1 in humans. ^{11}C-AS2471907 has reasonable brain uptake and high specific binding signals in the human brain. Imaging data are modeled well with the 2TC model, and model-derived regional V_T values display fairly good within-subject test-retest reproducibility. Nonetheless, between-subject variations in regional V_T values are large, which may be due to physiological differences among the subjects. In conclusion, ^{11}C-AS2471907 appears to be an appropriate radiotracer to image and quantify 11β-HSD1 in the human brain and can be used to assess enzyme occupancy of 11β-HSD1 inhibitors. However, accurate quantification of 11β-HSD1 under disease conditions may require the development of a radiotracer with better imaging characteristics.

DISCLOSURE

Mark Walzer and Gerard J. Marek are employees of Astellas; Susan Bellaire and Nancy Yuan were employees of Astellas at the time of the study. This study was funded by Astellas. No other potential conflicts of interest relevant to this article exist.

REFERENCES

1. Lakshmi V, Sakai RR, McEwen BS, Monder C. Regional distribution of 11 beta-hydroxysteroid dehydrogenase in rat brain. *Endocrinology.* 1991;128:1741-1748.

2. Moisan MP, Seckl JR, Brett LP, et al. 11beta-hydroxysteroid dehydrogenase messenger ribonucleic acid expression, bioactivity and immunoreactivity in rat cerebellum. *J Neuroendocrinol.* 1990;2:853-858.

3. Moisan MP, Seckl JR, Edwards CR. 11 beta-hydroxysteroid dehydrogenase bioactivity and messenger RNA expression in rat forebrain: localization in hypothalamus, hippocampus, and cortex. *Endocrinology.* 1990;127:1450-1455.

4. Seckl JR, Dow RC, Low SC, Edwards CR, Fink G. The 11 beta-hydroxysteroid dehydrogenase inhibitor glycyrrhetinic acid affects corticosteroid feedback regulation of hypothalamic corticotrophin-releasing peptides in rats. *J Endocrinol.* 1993;136:471-477.

5. Sandeep TC, Yau JL, MacLullich AM, et al. 11beta-hydroxysteroid dehydrogenase inhibition improves cognitive function in healthy elderly men and type 2 diabetics. *Proc Natl Acad Sci U S A.* 2004;101:6734-6739.

6. Harris HJ, Kotelevtsev Y, Mullins JJ, Seckl JR, Holmes MC. Intracellular regeneration of glucocorticoids by 11beta-hydroxysteroid dehydrogenase (11beta-HSD)-1 plays a key role in regulation of the hypothalamic-pituitary-adrenal axis: analysis of 11beta-HSD-1-deficient mice. *Endocrinology.* 2001;142:114-120.

7. Swaab DF, Bao AM, Lucassen PJ. The stress system in the human brain in depression and neurodegeneration. *Ageing Res Rev.* 2005;4:141-194.

8. Sinha R. Chronic stress, drug use, and vulnerability to addiction. *Ann N Y Acad Sci.* 2008;1141:105-130.

9. Stephens MA, Wand G. Stress and the HPA axis: role of glucocorticoids in alcohol dependence. *Alcohol Res.* 2012;34:468-483.

10. Meaney MJ, O'Donnell D, Rowe W, et al. Individual differences in hypothalamic-pituitary-adrenal activity in later life and hippocampal aging. *Exp Gerontol.* 1995;30:229-251.

11. Holmes MC, Carter RN, Noble J, et al. 11beta-hydroxysteroid dehydrogenase type 1 expression is increased in the aged mouse hippocampus and parietal cortex and causes memory impairments. *J neurosci.* 2010;30:6916-6920.

12. Holmes MC, Seckl JR. The role of 11beta-hydroxysteroid dehydrogenases in the brain. *Mol Cell Endocrinol.* 2006;248:9-14.

13. Mohler EG, Browman KE, Roderwald VA, et al. Acute inhibition of 11beta-hydroxysteroid dehydrogenase type-1 improves memory in rodent models of cognition. *J neurosci.* 2011;31:5406-5413.

14. Yau JL, McNair KM, Noble J, et al. Enhanced hippocampal long-term potentiation and spatial learning in aged 11beta-hydroxysteroid dehydrogenase type 1 knock-out mice. *J neurosci.* 2007;27:10487-10496.

15. Yau JL, Noble J, Kenyon CJ, et al. Lack of tissue glucocorticoid reactivation in 11beta -hydroxysteroid dehydrogenase type 1 knockout mice ameliorates age-related learning impairments. *Proc Natl Acad Sci U S A.* 2001;98:4716-4721.

16. Sooy K, Webster SP, Noble J, et al. Partial deficiency or short-term inhibition of 11beta-hydroxysteroid dehydrogenase type 1 improves cognitive function in aging mice. *J neurosci.* 2010;30:13867-13872.

17. Sooy K, Noble J, McBride A, et al. Cognitive and disease-modifying effects of 11ss-hydroxysteroid dehydrogenase type 1 inhibition in male Tg2576 mice, a model of Alzheimer's disease. *Endocrinology.* 2015;156:4592-4603.

18. Yarchoan M, Arnold SE. Repurposing diabetes drugs for brain insulin resistance in Alzheimer disease. *Diabetes.* 2014;63:2253-2261.

19. Li W, Joshi A, Zeng Z, et al. Radiosynthesis and evaluation of an 11-beta hydroxysteroid dehydrogenase-1 (11β-HSD1) PET ligand in rhesus monkey. *J Labelled Compd Radiopharm.* 2011;54:S293.

20. Kiso T, Sekizawa T, Uchino H, Tsukamoto M, Kakimoto S. Analgesic effect of ASP3662, a novel 11β-HSD1 inhibitor, in rat models of neuropathic and dysfunctional pain. *Br J Pharmacol.* 2018. [Epub ahead of print]

21. Hannestad J, Dellagioia N, Gallezot J-D, et al. The neuroinflammation marker translocator protein is not elevated in individuals with mild-to-moderate depression: a [^{11}C]PBR28 PET study. *Brain Behav Immun.* 2013;33:131-138.

22. Lin S-F, Labaree D, Chen M-K, et al. Further evaluation of [11C]MP-10 as a radiotracer for phosphodiesterase 10A: PET imaging study in rhesus monkeys and brain tissue metabolite analysis. *Synapse.* 2015;69:86-95.

23. Naganawa M, Waterhouse RN, Nabulsi NB, et al. First in human assessment of the novel PDE2A PET radiotracer 18F-PF-05270430. *J Nucl Med.* 2016;57:1388-1395.

24. Tzourio-Mazoyer N, Landeau B, Papathanassiou D, et al. Automated anatomical labeling of activations in SPM using a macroscopic anatomical parcellation of the MNI MRI single-subject brain. *Neuroimage.* 2002;15:273-289.

25. Innis RB, Cunningham VJ, Delforge J, et al. Consensus nomenclature for in vivo imaging of reversibly binding radioligands. *J Cereb Blood Flow Metab.* 2007;27:1533-1539.

26. Gunn RN, Gunn SR, Cunningham VJ. Positron emission tomography compartmental models. *J Cereb Blood Flow Metab.* 2001;21:635-652.

27. Cunningham VJ, Rabiner EA, Slifstein M, Laruelle M, Gunn RN. Measuring drug occupancy in the absence of a reference region: the Lassen plot re-visited. *J Cereb Blood Flow Metab.* 2010;30:46-50.

28. Shrout PE, Fleiss JL. Intraclass correlations: uses in assessing rater reliability. *Psychol Bull.* 1979;86:420-428.

29. Huang Y, Hwang D-R, Bae S-A, et al. A new positron emission tomography imaging agent for the serotonin transporter: synthesis, pharmacological characterization, and kinetic analysis of [11C]2-[2-(dimethylaminomethyl)phenylthio]-5-fluoromethylphenylamine ([11C]AFM). *Nucl Med Biol.* 2004;31:543-556.

30. Carson RE. PET physiological measurements using constant infusion. *Nucl Med Biol.* 2000;27:657-660.

31. Edwards S, Evans P, Hucklebridge F, Clow A. Association between time of awakening and diurnal cortisol secretory activity. *Psychoneuroendocrinology.* 2001;26:613-622.

TABLES

Table 1: Regional volumes of distribution (V_T, mL/cm^3) for ^{11}C-AS2471907 in baseline scans

	2TC	1TC
Caudate Nucleus	3.7 ± 1.5	3.1 ± 1.5
Amygdala	4.3 ± 1.9	3.7 ± 1.9
Centrum Semiovale	4.6 ± 1.6	3.6 ± 1.2
Cingulum	6.7 ± 2.6	5.9 ± 2.4
Insula	6.8 ± 2.8	5.9 ± 2.5
Frontal Cortex	8.9 ± 3.6	8.1 ± 3.4
Putamen	9.3 ± 3.7	8.7 ± 3.8
Temporal Cortex	9.4 ± 4.0	8.6 ± 3.8
Parietal Cortex	11.0 ± 4.3	10.3 ± 4.2
Cerebellum	11.4 ± 5.9	10.7 ± 5.8
Thalamus	11.9 ± 5.0	11.5 ± 5.0
Occipital Cortex	14.5 ± 5.3	13.5 ± 5.1

n=15

Table 2: Test-Retest Variability of ^{11}C-AS2471907 Volumes of Distribution (V_T)

	2TC		1TC	
	TRV	ICC	TRV	ICC
Caudate Nucleus	12% ± 22%	0.746	15% ± 8%	0.937
Amygdala	-7% ± 51%	0.691	1% ± 42%	0.800
Centrum Semiovale	11% ± 28%	0.546	16% ± 20%	0.799
Cingulum	17% ± 8%	0.853	17% ± 14%	0.868
Insula	14% ± 9%	0.883	11% ± 18%	0.900
Frontal Cortex	10% ± 7%	0.963	11% ± 14%	0.927
Putamen	10% ± 14%	0.919	11% ± 17%	0.908
Temporal Cortex	14% ± 8%	0.928	13% ± 12%	0.934
Parietal Cortex	13% ± 13%	0.821	13% ± 11%	0.897
Cerebellum	9% ± 14%	0.977	10% ± 15%	0.979
Thalamus	12% ± 20%	0.614	12% ± 11%	0.831
Occipital Cortex	11% ± 5%	0.940	10% ± 7%	0.962

n=5

FIGURES

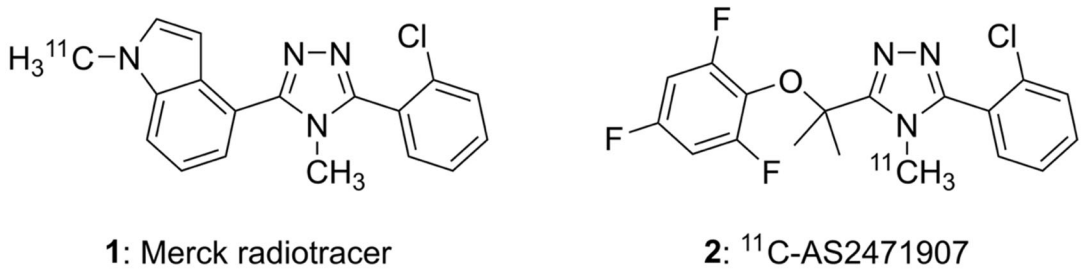

1: Merck radiotracer

2: ^{11}C-AS2471907

Figure 1: Chemical structures of radiotracers for 11β-HSD1

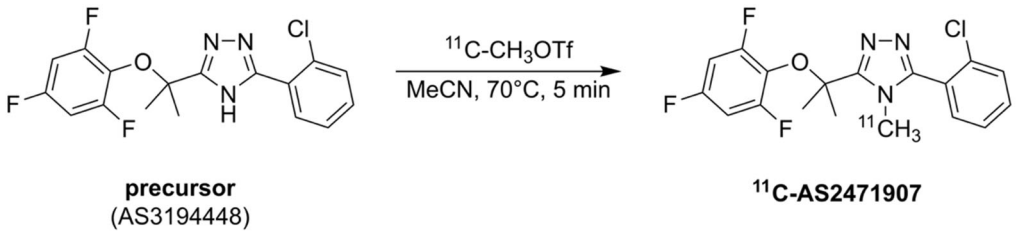

Figure 2: Radiosynthesis of ^{11}C-AS2471907.

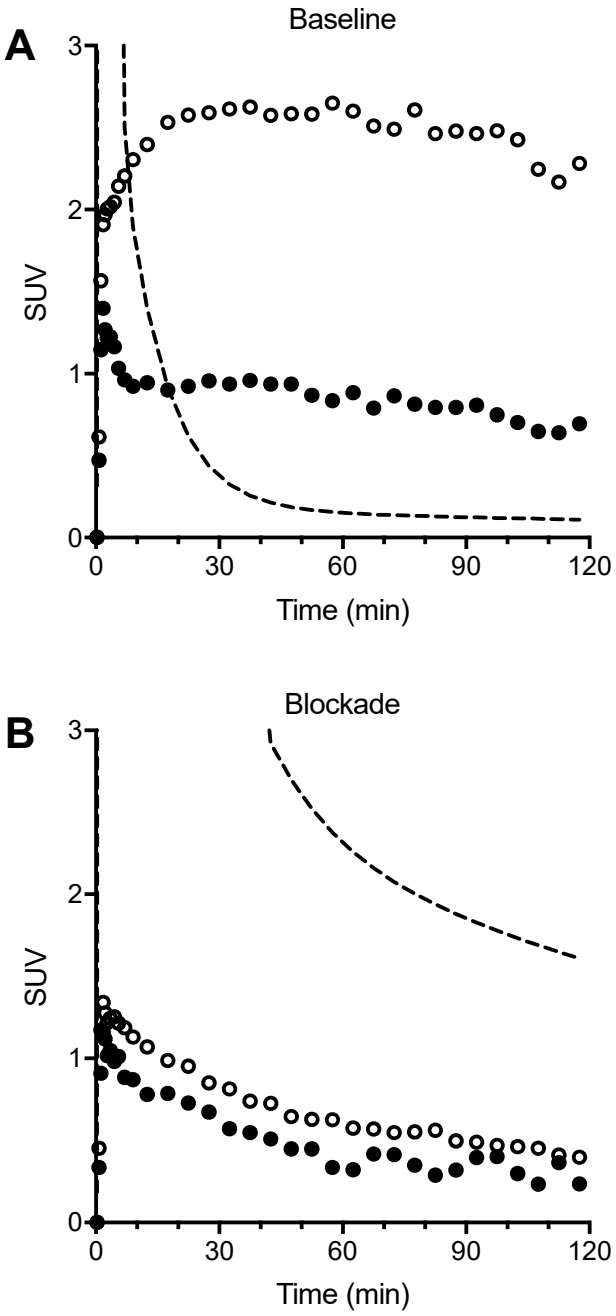

Figure 3: Regional time-activity curves at baseline (**A**) and after ASP3662 administration (**B**) in the occipital cortex (open circles) and caudate (solid circles). The dashed lines represent the metabolite-corrected input function. SUV: standardized uptake value.

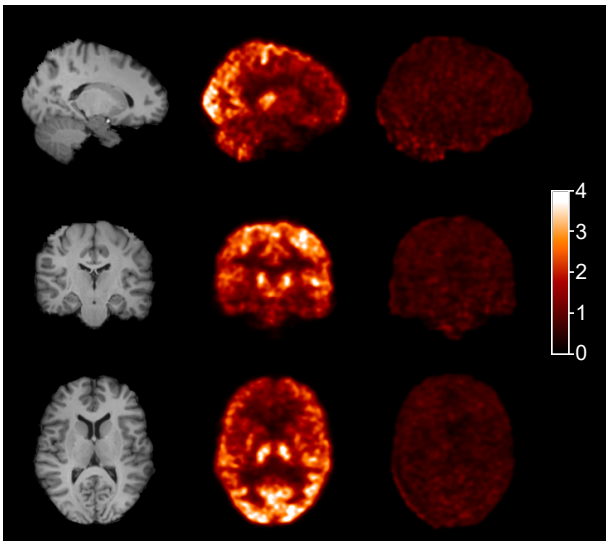

Figure 4: MRI (left) and baseline (center) and post-drug (right) PET standard uptake value images (SUV, averaged from 40-60 min).

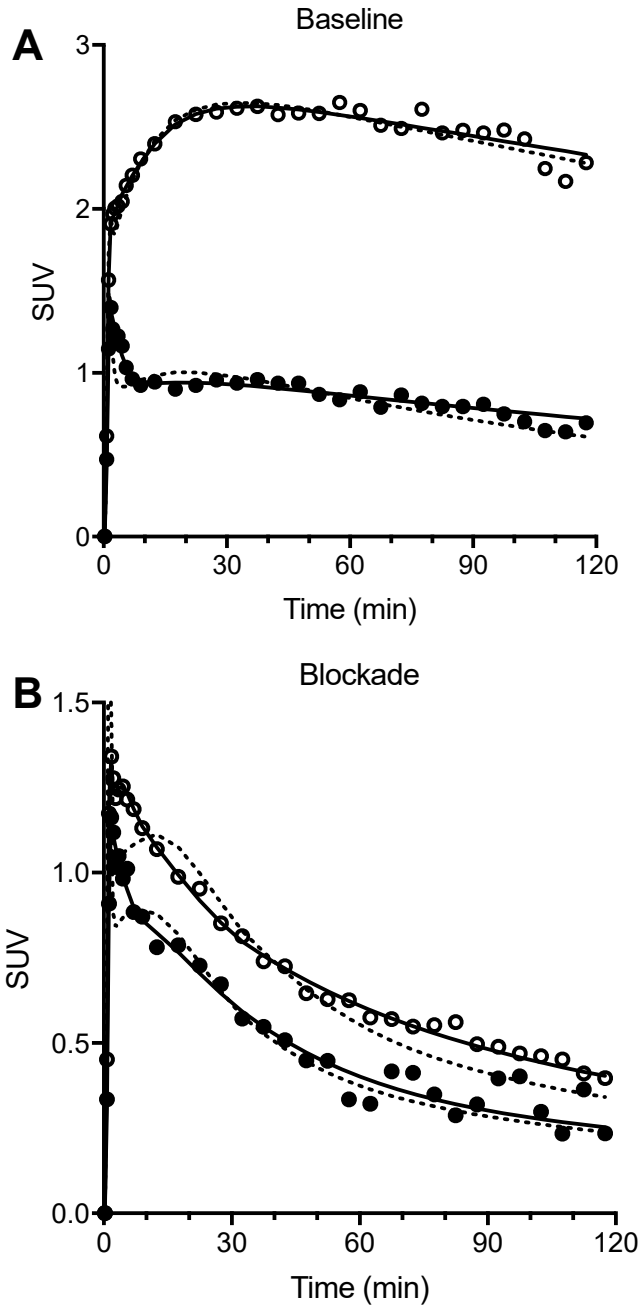

Figure 5: Regional time-activity curves and fitted curves at baseline (**A**) and after ASP3662 administration (**B**) in the occipital cortex (open circles) and caudate (solid circles). The solid lines represent 2TC model fits, and the dotted lines represent the 1TC model fits. SUV: standardized uptake value.

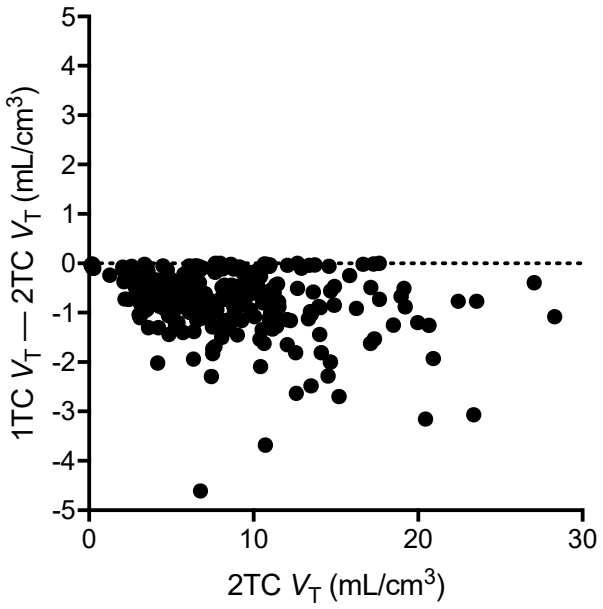

Figure 6: Bland-Altman plot of V_T values from the 2TC and 1TC models.

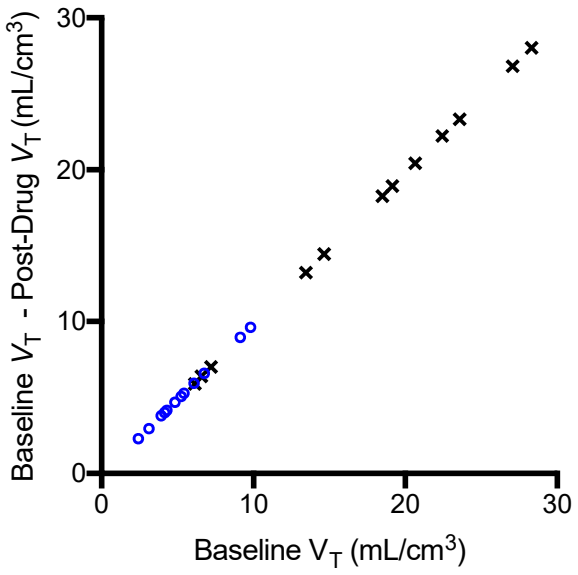

Figure 7: Occupancy plots for the two blockade studies. The occupancy was estimated to be >99% for both studies, and the non-displaceable volume of distribution (V_{ND}) was estimated to be 0.19 ± 0.016 mL/cm^3 in the first subject (black cross symbols) and 0.13 ± 0.011 mL/cm^3 in the second subject (blue circles).

SUPPLEMENTAL DATA

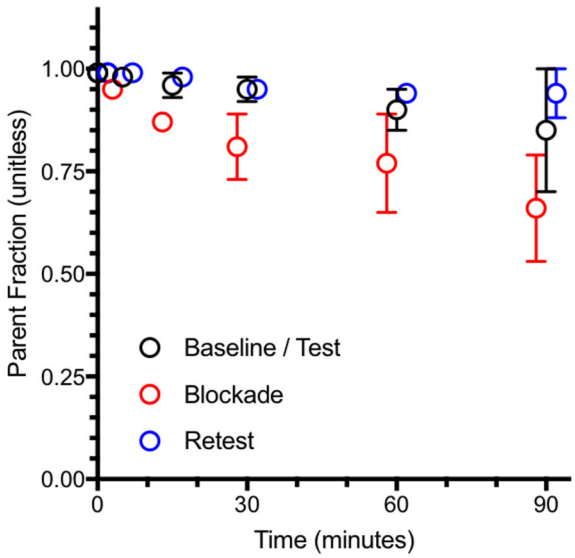

Supplemental Figure 1: Parent fraction in plasma for the baseline or test scans (n=15, black), blockade scans (n=2, red), and retest scans (n=5, blue). Data are presented as mean ± SD. Error bars are not shown if they are shorter than the symbol used to show the mean.

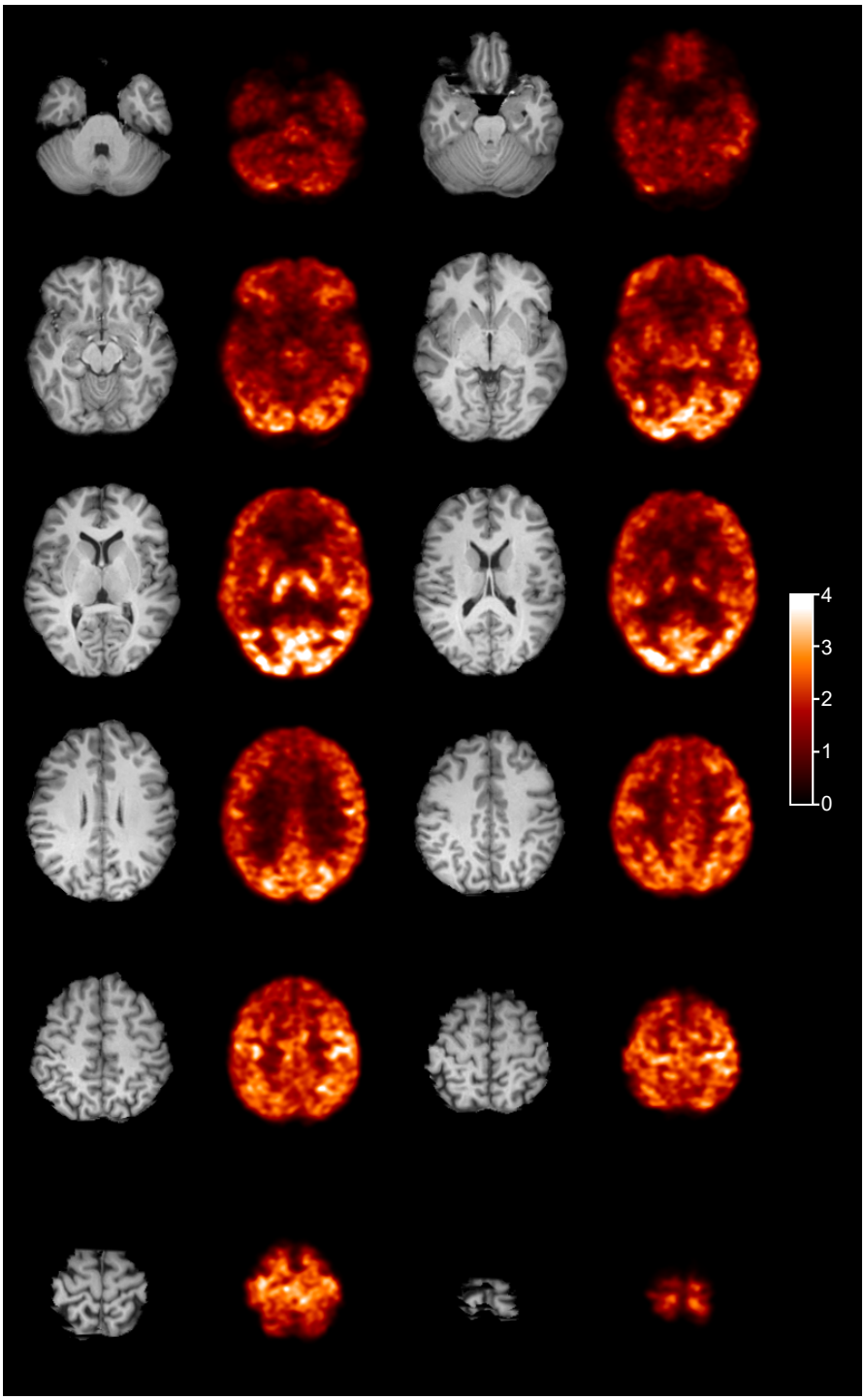

Supplemental Figure 2: Transverse PET slices from a baseline ^{11}C-AS2471907 scan, shown as standard uptake values (SUV, averaged from 40-60 min post injection). Corresponding MR images are shown to the left-hand side of each PET image.

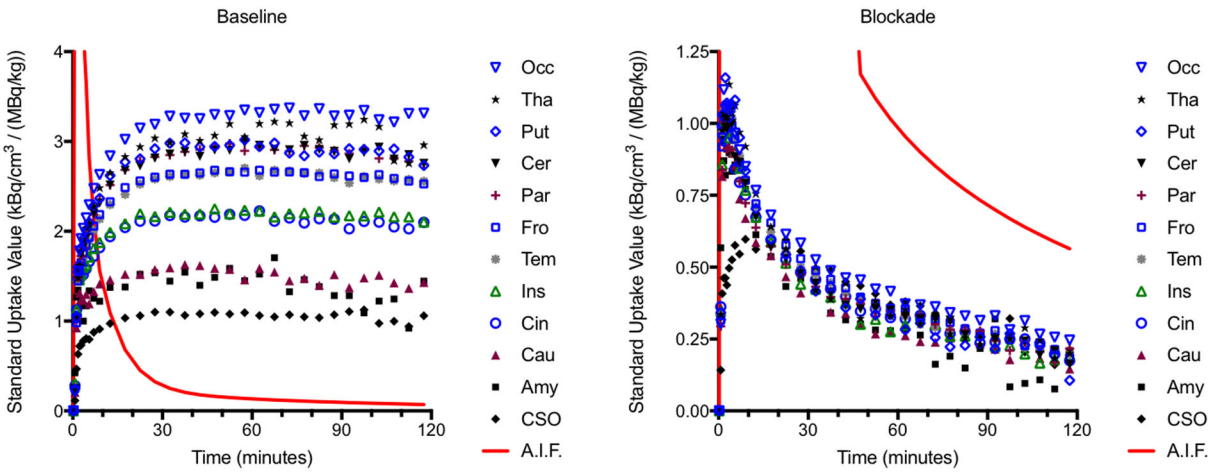

Supplemental Figure 3: Representative brain time-activity curves at baseline and after pre-blockade of 11β-HSD1 binding sites with ASP3662. Occ = Occipital Cortex, Tha = Thalamus, Put = Putamen, Cer = Cerebellum, Par = Parietal Cortex, Fro = Frontal cortex, Tem = Temporal cortex, Ins = Insula, Cin = Cingulum, Cau = Caudate Nucleus, Amy = Amygdala, CSO = Centrum Semiovale, A.I.F. = Metabolite-Corrected Arterial input function.

Supplemental Table 1: 2TC V_T values estimated for the baseline and blockade scans.

	Subject 6		Subject 7	
	Baseline	Blockade	Baseline	Blockade
Caudate Nucleus	7.2	0.20	2.4	0.13
Amygdala	6.6	0.17	4.2	0.16
Centrum Semiovale	6.1	0.25	3.1	0.18
Cingulum	13.4	0.22	4.3	0.15
Insula	14.7	0.22	3.9	0.15
Frontal Cortex	18.5	0.24	5.3	0.17
Putamen	19.1	0.22	6.1	0.15
Temporal Cortex	20.7	0.23	5.4	0.16
Parietal Cortex	22.4	0.23	6.8	0.18
Cerebellum	23.6	0.24	4.8	0.14
Thalamus	27.1	0.25	9.1	0.16
Occipital Cortex	28.3	0.28	9.8	0.19

Supplemental Table 2: 2TC V_T values estimated from the test and retest scans.

Subject	Scan	Injection Time	CSO	Amy	Cau	Put	Tha	Cer	Cin	Ins	Fro	Occ	Par	Tem
1	T	10:46	6.8	3.1	3.6	7.1	13.5	6.1	5.2	4.9	6.4	11.1	10.4	6.2
1	R	15:43	4.8	2.4	3.4	9.5	11.0	5.8	6.9	5.7	7.4	11.4	10.5	7.4
2	T	10:47	5.0	4.3	4.2	9.5	9.6	5.8	6.8	6.7	9.0	14.9	11.1	9.0
2	R	17:12	7.5	3.5	4.7	10.7	12.7	7.7	8.1	8.7	10.4	17.7	12.9	11.5
3	T	12:18	4.9	8.2	6.6	11.3	15.8	19.0	8.8	8.2	12.2	20.9	14.9	13.3
3	R	16:44	5.4	5.2	10.7	11.3	17.6	20.0	9.3	8.8	12.6	23.4	20.4	14.1
4	T	09:48	2.3	1.3	2.2	4.4	9.2	6.5	3.4	3.5	4.4	7.8	5.5	4.7
4	R	14:50	3.1	3.0	2.1	5.2	12.6	6.4	4.2	4.1	5.0	9.0	6.7	5.4
5	T	15:02	4.5	7.8	3.6	13.4	14.6	8.6	7.7	8.1	11.0	17.3	13.7	10.8
5	R	17:45	5.0	5.8	4.0	12.7	16.3	10.3	9.0	8.5	11.3	19.2	13.6	11.5

T = Test, R = Retest, CSO = Centrum Semiovale, Amy = Amygdala, Cau = Caudate Nucleus, Put = Putamen, Tha = Thalamus, Cer = Cerebellum, Cin = Cingulum, Ins = Insula, Fro = Frontal cortex, Occ = Occipital Cortex, Par = Parietal Cortex, Tem = Temporal cortex.

Supplemental Table 3: Bias* on 2TC V_T values estimated with shorter scan length.

Scan length (min)	60	70	80	90	100	110
Caudate Nucleus	817%±3592%	39%±110%	13%±23%	11%±19%	9%±12%	5%±5%
Amygdala	12%±61%	9%±39%	6%±25%	7%±16%	5%±9%	4%±5%
Centrum Semiovale	12%±40%	8%±18%	9%±14%	6%±9%	4%±6%	2%±3%
Cingulum	5%±12%	6%±11%	5%±8%	5%±6%	4%±4%	2%±3%
Insula	4%±13%	6%±10%	5%±7%	5%±6%	4%±5%	2%±2%
Frontal Cortex	2%±12%	3%±9%	3%±7%	4%±5%	3%±4%	2%±2%
Putamen	7%±30%	7%±18%	4%±13%	3%±9%	4%±7%	2%±4%
Temporal Cortex	5%±16%	8%±14%	8%±11%	7%±9%	4%±5%	2%±3%
Parietal Cortex	9%±17%	8%±12%	8%±11%	7%±8%	4%±5%	2%±2%
Cerebellum	11%±29%	15%±26%	11%±20%	9%±17%	6%±9%	4%±4%
Thalamus	3%±12%	4%±11%	5%±8%	5%±7%	3%±4%	2%±3%
Occipital Cortex	28%±34%	23%±24%	17%±17%	14%±12%	10%±8%	5%±3%

* bias computed as $V_{\mathrm{T}}^{Scan\ length} / V_{\mathrm{T}}^{120\ \mathrm{min}} - 1$; bias presented as mean ± standard deviation.